

Electronic Supplementary Information

**Pore modulation of zirconium–organic frameworks for high-efficiency
detection of trace protein**

Chun-Sen Liu,[†] Zhi-Hong Zhang,[†] Min Chen, Hui Zhao, Feng-He Duan, Di-Ming Chen,
Ming-Hua Wang, Shuai Zhang and Miao Du*

*Henan Provincial Key Lab of Surface & Interface Science, Zhengzhou University of
Light Industry, Zhengzhou 450002, P. R. China*

[†] These authors contributed equally.

* E-mail: dumiao@zzuli.edu.cn.

Chem. Commun.

Experimental section

Materials. The ligand 4,4',4''-s-triazine-2,4,6-tribenzoic acid (H₃TATB) was prepared according to literature method^{S1} and other chemicals for MOFs synthesis were commercially available. Biologicals including aptamer (5'-NH₂-ATCAGGGCTAAAGAGTGCAGAGTTACTTAG-3'), lysozyme, platelet-derived growth factor-BB (PDGF-BB), bovine serum albumin (BSA), thrombin, immunoglobulin G (IgG) and immunoglobulin E (IgE) were ordered from Beijing SBS Genetech Co., Ltd.

Physical measurements. Elemental analyses of C, H, and N were performed on a Vario EL III Elementar analyzer. IR spectra were measured on a Bruker Tensor 27 OPUS FT-IR spectrometer with KBr pellets in 4000–400 cm⁻¹. Powder X-ray diffraction (PXRD) patterns were recorded on a Rigaku (model Ultima IV) diffractometer, equipped with a Rigaku D/teX ultrahigh-speed position sensitive detector and Cu-K α X-ray (40 kV and 40 mA). The intensity data were collected in step-scan mode with the scan rate of 2 °/min and step size of 0.02°. Thermogravimetric analysis (TGA) was performed on a Perkin-Elmer Diamond SII thermal analyzer from room temperature to 800 °C, with a heating rate of 10 °C min⁻¹ under N₂ atmosphere. Gas sorption isotherms were taken on a Micromeritics 3Flex surface area and pore size analyzer under ultrahigh vacuum in a clean system. Ultrahigh-purity-grade (> 99.999%) N₂, CO₂, H₂ and He gases were applied in all measurements. The experimental temperatures were maintained by liquid nitrogen (77 K), liquid argon (87 K), and the temperature-programmed water bath (273 and 293 K). X-ray photoelectron spectroscopy (XPS) data were acquired using an AXIS HIS 165 spectrometer with a monochromatized Al-Kr X-ray source (1486.71 eV photons).

Syntheses of 493-MOFs. For 493-MOF-BA, a mixture of ZrOCl₂·8H₂O (64.5 mg, 0.2 mmol), benzoic acid (30.5 mg, 2.5 mmol), acetic acid (1 mL), and DMF (3 mL) was ultrasonically dissolved in a vial (10 mL), which was sealed into a Teflon-lined stainless steel vessel and heated at 80 °C for 2 h in an oven. Then, H₃TATB (22.1 mg, 0.05 mmol) was added, which was heated at

120 °C for 72 h. After cooling to room temperature, colorless octahedral crystals were collected and washed with fresh DMF for three times. Yield: 41.3 mg (53% based on H₃TATB). IR (cm⁻¹): 3422b, 1676vs, 1607m, 1567m, 1518m, 1357s, 1253m, 1174w, 1139w, 1091m, 1016m, 886w, 773m, 724m, 700m, 491m, 417w. Anal. Calcd (%) for {[Zr₆(μ₃-O)₄(μ₃-OH)₄(OH)₄(BA)(H₂O)₄(OAc)(TATB)₂](DMF)₁₆(H₂O)₄}_n (C₁₀₅H₁₆₈N₂₂O₅₂Zr₆): C, 40.45; H, 5.43; N, 9.88. Found (%): C, 40.66; H, 5.46; N, 9.85. 493-MOF-NA was obtained by a similar procedure used for synthesis of 493-MOF-BA, in which benzoic acid was replaced by nicotinic acid (30.8 mg, 2.5 mmol). Yield: 46.0 mg (59% based on H₃TATB). IR (cm⁻¹): 3413b, 1658vs, 1608m, 1566m, 1518m, 1403s, 1358m, 1253m, 1160w, 1139w, 1097m, 1016m, 885w, 798m, 774m, 700m, 493m. Anal. Calcd (%) for {[Zr₆(μ₃-O)₄(μ₃-OH)₄(OH)₄(NA)(H₂O)₄(OAc)(TATB)₂](DMF)₁₆(H₂O)₄}_n (C₁₀₄H₁₆₇N₂₃O₅₂Zr₆): C, 40.05; H, 5.40; N, 10.33. Found (%): C, 40.03; H, 5.43; N, 10.64. Also, 493-MOF-TATB was similarly prepared, except that benzoic acid (30.5 mg, 2.5 mmol) was replaced by tetrahydrofuran-2-carboxylic acid (29.0 mg, 2.5 mmol). Yield: 23.2 mg (45% based on H₃TATB). IR (cm⁻¹): 3420b, 1655s, 1611s, 1565s, 1504m, 1402vs, 1358s, 1096w, 1014w, 885w, 823w, 774s, 700w, 651m, 500m, 418w. Anal. Calcd (%) for {[Zr₆(μ₃-O)₄(μ₃-OH)₄(OH)₂(H₂O)₄(OAc)(TATB)₃](DMF)₁₀(H₂O)₁₁}_n (C₁₀₄H₁₄₅N₁₉O₅₅Zr₆): C, 40.44; H, 4.73; N, 8.62. Found (%): C, 40.45; H, 4.61; N, 8.74.

Single crystal X-ray crystallography. Diffraction data were collected on an Oxford Xcalibur Gemini Eos diffractometer with graphite-monochromated Cu-Kα radiation (λ = 1.5418 Å). Multi-scan absorption corrections were taken using the *CrysAlisPro* program.^{S2} Empirical absorption corrections were carried out with spherical harmonics, implemented in *SCALE3 ABSPACK* scaling algorithm. The crystal structures were solved by direct methods and all non-hydrogen atoms were refined anisotropically by full-matrix least-squares method with *SHELXTL* software package.^{S3} The C-bound H atoms were located geometrically and refined isotropically as ridings for the coordination frameworks, while hydrogen atoms of hydroxide and water were not determined.

Attempts to locate and model the highly disordered solvent molecules in the pores were unsuccessful. Therefore, the SQUEEZE routine, a part of the *PLATON* software package, was used to calculate the disorder areas and remove the diffraction contribution to afford a set of solvent free diffraction intensity.^{S4} The chemical formulas for MOFs were determined based on crystal data combined with the result of elemental and thermogravimetric analysis. Crystallographic data and structural refinement details were shown in Table S1, and selected bond lengths and angles were listed in Table S2.

Activation of 493-MOFs. The as-synthesized 493-MOF (ca. 120 mg) was soaked in CH₂Cl₂ (50 mL) for 12 h and the extract was discarded. Subsequently, fresh CH₂Cl₂ (50 mL) was added and the sample was allowed to soak for another 12 h. This refilling-and-removing cycle was repeated three times. The sample was transferred to a pre-weighed sample tube, evacuated (< 10⁻³ torr) at room temperature for 30 min, then dried using the outgas function of the sorption instrument for 12 h at 60 °C before gas adsorption and desorption measurements.

Fabrication of 493-MOF-based aptasensors. The crystal sample of 493-MOF was grinded to powders, following by dispersing into deionized water with a concentration of 1 mg mL⁻¹. Then, the homogeneous dispersion (5 μL) was dropped onto the surface of a bare gold electrode. Such a gold electrode modified by 493-MOF was incubated in aptamer (100 nM) for 2 h. Subsequently, the electrode was gently washed with phosphate buffer solution and dried in nitrogen atmosphere, affording 493-MOF-modified aptasensor used for electrochemical measurement. Notably, this is the optimized condition for fabrication of aptasensor, where too large amount of Zr-MOFs dispersion would peel off from the electrode surface, while too little amount of Zr-MOFs dispersion could not fully cover the electrode surface.

Electrochemical impedance spectroscopy (EIS) measurements. The bare gold electrode was polished with water slurries of fine alumina power (0.3 and 0.05 μm), following by rinsed with fresh piranha solution (1:3 mixture of 30% H₂O₂ and H₂SO₄) for 10 min. After that, the electrode

was ultra-sonicated in water and anhydrous ethanol. Phosphate buffer solution (PBS) (pH = 7.4) was prepared by mixing Na₂HPO₄ (0.067 M) and KH₂PO₄ (0.067 M) in the volume ratio of 8:2, which was used for the preparation of solutions of aptamer and proteins. The electrolyte solution was prepared immediately before use, by dissolving K₃[Fe(CN)₆] (1.65 g), K₄[Fe(CN)₆] (2.11 g), NaCl (8 g), and KCl (0.2 g) in PBS (1 L). The lysozyme stock solution was dissolved in PBS at a concentration of 1 mg mL⁻¹.

Lysozyme detection by electrochemical measurements. The 493-MOF-based aptasensor was placed in a three electrode cell, with a modified gold electrode (diameter: 3 mm) as the working electrode, a platinum wire as the counter electrode, and an Ag/AgCl electrode (saturated KCl) as the reference electrode. The measured potentials were reported with regard to the reference electrode. EIS measurements were taken in Fe(CN)₆^{3-/4-} (5.0 mM), in the frequency range of 0.01–1 MHz with 25 mV amplitude under the open circuit potential using a CHI 660E Electrochemical Workstation. All electrochemical experiments were carried out at room temperature (25 ± 1 °C) and each experiment was conducted at least in triplicate.

For control, the prepared biosensor was immersed in different interfere proteins for 2 h and the resulting EIS results were analyzed using Zview2 software. A nonlinear least-squares fitting was taken to determine the elemental parameters in the equivalent circuit. The semicircle portion at higher frequencies corresponds to the transfer limited process while the linear portion at lower frequencies corresponds to the diffusion process. The Randles equivalent circuit consists of solution resistance (R_s), charge transfer resistance (R_{ct}) as the diameter of semicircle, constant-phase element (CPE), and Warburg impedance (W_o). The concentration of lysozyme was quantified by a decrease in electron transfer resistance ΔR_{ct} ($R_{ct,0} - R_{ct,i}$), in which $R_{ct,0}$ and $R_{ct,i}$ are the electron transfer resistance in the absence and presence of lysozyme, respectively.

Simulation details. The structure of aptamer was generated using chembio3D and the geometry was optimized with Forcite module in material studio 6.1. The structures of Zr-MOFs were taken

directly from the crystal data. To simulate the interaction between the aptamer and the MOF surface, the structure of MOF was treated by cleave surface operation along the c axis with an equal thickness. The Adsorption Locator module was used to evaluate the binding details between the aptamer and the MOF surface. During the simulated annealing procedure, the quality was set to ultra-fine and the loading was set to one. The temperature was automatically controlled and UFF forcefield was applied. The QEq method was used to calculate the charges for the MOFs and the aptamer.

Table S1 Crystallographic data and structural refinement details.

	493-MOF-BA	493-MOF-TATB
Empirical formula	C ₁₀₅ H ₁₆₈ N ₂₂ O ₅₂ Zr ₆	C ₁₀₄ H ₁₄₅ N ₁₉ O ₅₅ Zr ₆
Formula weight	3117.92	3088.70
Crystal system	tetragonal	tetragonal
Space group	<i>I</i> -42 <i>d</i>	<i>I</i> -42 <i>d</i>
<i>a</i> / Å	38.8511(3)	38.9025(7)
<i>b</i> / Å	38.8511(3)	38.9025(7)
<i>c</i> / Å	18.7521(8)	18.9223(11)
Volume / Å ³	28304.6(13)	28637.1(19)
<i>Z</i>	8	8
<i>D</i> / g cm ⁻³	1.463	1.433
μ / mm ⁻¹	4.267	4.220
<i>F</i> (000)	7456	8464
<i>R</i> _{int}	0.0540	0.0582
<i>R</i> ₁ ^{<i>a</i>} / <i>wR</i> ₂ ^{<i>b</i>} [<i>I</i> > 2σ(<i>I</i>)]	0.0494 / 0.1159	0.0558 / 0.1513
<i>R</i> ₁ ^{<i>a</i>} / <i>wR</i> ₂ ^{<i>b</i>} (all data)	0.0934 / 0.1422	0.0648 / 0.1611
CCDC number	1501750	1501751

^{*a*} $R_1 = \sum ||F_o| - |F_c|| / \sum |F_o|$. ^{*b*} $wR_2 = [\sum w(|F_o|^2 - |F_c|^2)|^2]^{1/2} / [\sum w(F_o^2)]^{1/2}$, where $w = 1 / [\sigma^2(F_o^2) + (aP)^2 + bP]$ and $P = (F_o^2 + 2F_c^2) / 3$.

Table S2 Selected bond lengths (Å) and angles (°) for 493-MOF-BA and 493-MOF-TATB.

493-MOF-BA			
Zr1–O1	2.242(8)	Zr1–O3 ^{#2}	2.197(7)
Zr1–O7	2.131(8)	Zr1–O8 ^{#1}	2.166(8)
Zr1–O9	2.122(10)	Zr1–O10	2.144(8)
Zr1–O13	2.281(11)	Zr1–O14	2.242(10)
Zr2–O4 ^{#3}	2.223(7)	Zr2–O6 ^{#4}	2.193(9)
Zr2–O7	2.177(8)	Zr2–O8	2.125(8)
Zr2–O10	2.132(7)	Zr2–O10 ^{#1}	2.170(9)
Zr2–O12	2.203(7)	Zr2–O15	2.190(10)
Zr3–O2 ^{#1}	2.214(7)	Zr3–O5 ^{#4}	2.234(10)
Zr3–O7	2.156(8)	Zr3–O8	2.105(7)
Zr3–O9	2.134(9)	Zr3–O9 ^{#1}	2.227(12)
Zr3–O11	2.180(9)	Zr3–O16	2.238(10)
O7–Zr1–O8 ^{#1}	109.0(4)	O9–Zr1–O10	110.3(3)
O3 ^{#2} –Zr1–O13	115.5(4)	O1–Zr1–O14	117.0(4)
O9–Zr1–O14	140.6(4)	O7–Zr1–O1	140.9(3)
O7–Zr1–O3 ^{#2}	142.4(3)	O10–Zr1–O1	142.5(4)
O9–Zr1–O3 ^{#2}	142.7(4)	O10–Zr1–O13	142.9(4)
O8 ^{#1} –Zr1–O13	143.7(3)	O8 ^{#1} –Zr1–O14	144.8(4)
O9–Zr1–O7	69.7(4)	O14–Zr1–O13	69.7(4)
O7–Zr1–O10	70.1(3)	O10–Zr1–O8 ^{#1}	70.8(3)
O9–Zr1–O8 ^{#1}	72.0(4)	O1–Zr1–O13	73.9(4)
O3 ^{#2} –Zr1–O14	75.3(3)	O9–Zr1–O1	76.3(3)
O3 ^{#2} –Zr1–O1	76.5(3)	O8 ^{#1} –Zr1–O1	77.0(4)
O8 ^{#1} –Zr1–O3 ^{#2}	77.4(3)	O10–Zr1–O3 ^{#2}	78.1(3)
O9–Zr1–O13	80.3(4)	O7–Zr1–O14	80.9(4)

O7-Zr1-O13	81.8(4)	O10-Zr1-O14	82.1(4)
O8-Zr2-O10	107.7(4)	O10 ^{#1} -Zr2-O7	108.1(4)
O6 ^{#4} -Zr2-O12	116.2(3)	O15-Zr2-O4 ^{#3}	116.9(4)
O7-Zr2-O4 ^{#3}	141.2(3)	O10 ^{#1} -Zr2-O6 ^{#4}	141.2(3)
O8-Zr2-O15	141.8(3)	O10-Zr2-O6 ^{#4}	142.4(3)
O10-Zr2-O4 ^{#3}	142.6(3)	O10 ^{#1} -Zr2-O15	143.7(3)
O7-Zr2-O12	143.9(3)	O8-Zr2-O12	144.1(3)
O10-Zr2-O10 ^{#1}	69.0(3)	O10-Zr2-O7	69.4(3)
O8-Zr2-O7	69.5(3)	O8-Zr2-O10 ^{#1}	71.0(3)
O15-Zr2-O12	72.2(4)	O12-Zr2-O4 ^{#3}	74.0(3)
O15-Zr2-O6 ^{#4}	74.7(4)	O6 ^{#4} -Zr2-O4 ^{#3}	75.0(3)
O8-Zr2-O6 ^{#4}	75.8(3)	O8-Zr2-O4 ^{#3}	77.5(3)
O7-Zr2-O6 ^{#4}	77.7(3)	O10 ^{#1} -Zr2-O4 ^{#3}	78.5(3)
O7-Zr2-O15	80.9(4)	O10 ^{#1} -Zr2-O12	82.2(4)
O10-Zr2-O15	82.5(4)	O10-Zr2-O12	83.4(3)
O7-Zr3-O9 ^{#1}	109.9(4)	O8-Zr3-O9	110.1(4)
O2 ^{#1} -Zr3-O16	112.1(4)	O11-Zr3-O5 ^{#4}	119.0(3)
O9-Zr3-O5 ^{#4}	140.3(4)	O9 ^{#1} -Zr3-O5 ^{#4}	140.9(3)
O8-Zr3-O16	141.9(3)	O7-Zr3-O2 ^{#1}	142.0(3)
O8-Zr3-O11	142.8(3)	O7-Zr3-O11	143.1(3)
O9-Zr3-O2 ^{#1}	144.6(4)	O9 ^{#1} -Zr3-O16	145.6(4)
O9-Zr3-O7	69.0(4)	O8-Zr3-O7	70.2(3)
O8-Zr3-O9 ^{#1}	71.1(4)	O5 ^{#4} -Zr3-O16	72.1(4)
O9-Zr3-O9 ^{#1}	72.9(4)	O11-Zr3-O16	73.1(4)
O11-Zr3-O2 ^{#1}	74.2(4)	O2 ^{#1} -Zr3-O5 ^{#4}	74.7(3)
O8-Zr3-O5 ^{#4}	76.2(3)	O7-Zr3-O5 ^{#4}	77.4(3)
O2 ^{#1} -Zr3-O9 ^{#1}	78.2(4)	O8-Zr3-O2 ^{#1}	78.4(3)
O11-Zr3-O9 ^{#1}	78.9(4)	O9-Zr3-O11	80.5(4)
O7-Zr3-O16	82.6(4)	O9-Zr3-O16	82.9(4)

493-MOF-TATB

Zr1-O9	2.139(7)	Zr1-O11 ^{#1}	2.157(10)
Zr1-O9 ^{#1}	2.173(10)	Zr1-O12	2.185(10)
Zr1-O1	2.203(7)	Zr1-O4 ^{#2}	2.207(7)
Zr1-O10	2.207(9)	Zr1-O7	2.269(8)
Zr2-O9	2.101(9)	Zr2-O10	2.164(6)
Zr2-O15 ^{#1}	2.171(8)	Zr2-O11	2.172(10)
Zr2-O6 ^{#3}	2.209(7)	Zr2-O14	2.239(10)
Zr2-O2 ^{#1}	2.256(7)	Zr2-O13	2.258(10)
Zr3-O15	2.130(7)	Zr3-O11	2.136(11)
Zr3-O10 ^{#1}	2.144(8)	Zr3-O16	2.152(8)
Zr3-O15 ^{#1}	2.167(11)	Zr3-O5 ^{#3}	2.233(6)
Zr3-O8	2.244(8)	Zr3-O3 ^{#4}	2.279(8)
O9 ^{#1} -Zr1-O10	107.7(4)	O9-Zr1-O11 ^{#1}	108.5(5)
O12-Zr1-O1	114.1(4)	O4 ^{#2} -Zr1-O7	121.5(3)
O11 ^{#1} -Zr1-O7	139.2(4)	O1-Zr1-O10	140.7(3)
O9 ^{#1} -Zr1-O4 ^{#2}	141.5(3)	O9-Zr1-O4 ^{#2}	141.5(3)
O9-Zr1-O1	142.5(3)	O9 ^{#1} -Zr1-O12	143.8(3)
O11 ^{#1} -Zr1-O12	144.3(4)	O10-Zr1-O7	145.3(3)
O9-Zr1-O10	69.6(3)	O11 ^{#1} -Zr1-O10	69.6(4)
O9-Zr1-O9 ^{#1}	69.9(4)	O11 ^{#1} -Zr1-O9 ^{#1}	70.3(4)
O12-Zr1-O4 ^{#2}	73.7(3)	O1-Zr1-O7	73.9(3)
O12-Zr1-O7	74.7(4)	O1-Zr1-O4 ^{#2}	76.0(3)
O11 ^{#1} -Zr1-O1	76.4(4)	O9 ^{#1} -Zr1-O7	76.5(4)
O11 ^{#1} -Zr1-O4 ^{#2}	76.5(4)	O10-Zr1-O4 ^{#2}	77.3(3)
O9 ^{#1} -Zr1-O1	77.7(3)	O9-Zr1-O7	80.5(3)
O9-Zr1-O12	84.0(4)	O12-Zr1-O10	85.0(4)
O9-Zr2-O15 ^{#1}	108.6(4)	O10-Zr2-O11	110.9(4)

O14-Zr2-O2 ^{#1}	112.9(3)	O6 ^{#3} -Zr2-O13	116.0(4)
O15 ^{#1} -Zr2-O13	140.1(4)	O10-Zr2-O6 ^{#3}	140.8(3)
O9-Zr2-O14	141.6(4)	O9-Zr2-O6 ^{#3}	141.9(3)
O15 ^{#1} -Zr2-O2 ^{#1}	142.6(3)	O10-Zr2-O2 ^{#1}	143.1(3)
O11-Zr2-O13	145.8(4)	O11-Zr2-O14	146.0(4)
O14-Zr2-O13	65.1(4)	O10-Zr2-O15 ^{#1}	68.5(3)
O9-Zr2-O10	71.1(3)	O9-Zr2-O11	71.3(4)
O15 ^{#1} -Zr2-O11	71.7(4)	O6 ^{#3} -Zr2-O14	75.0(3)
O11-Zr2-O6 ^{#3}	75.8(3)	O6 ^{#3} -Zr2-O2 ^{#1}	75.9(3)
O11-Zr2-O2 ^{#1}	76.1(4)	O2 ^{#1} -Zr2-O13	76.3(4)
O9-Zr2-O2 ^{#1}	77.8(3)	O15 ^{#1} -Zr2-O6 ^{#3}	78.2(3)
O10-Zr2-O13	80.9(3)	O10-Zr2-O14	82.1(4)
O9-Zr2-O13	83.5(5)	O15 ^{#1} -Zr2-O14	85.4(5)
O16-Zr3-O5 ^{#3}	105.7(3)	O10 ^{#1} -Zr3-O15 ^{#1}	109.3(4)
O15-Zr3-O11	109.9(5)	O8-Zr3-O3 ^{#4}	123.0(3)
O15 ^{#1} -Zr3-O3 ^{#4}	141.3(3)	O11-Zr3-O8	141.7(4)
O10 ^{#1} -Zr3-O8	141.8(3)	O15-Zr3-O3 ^{#4}	142.1(3)
O15-Zr3-O5 ^{#3}	142.2(3)	O10 ^{#1} -Zr3-O5 ^{#3}	142.8(3)
O16-Zr3-O15 ^{#1}	143.5(3)	O11-Zr3-O16	144.0(4)
O15-Zr3-O15 ^{#1}	69.2(4)	O15-Zr3-O10 ^{#1}	69.6(3)
O16-Zr3-O8	70.2(3)	O11-Zr3-O10 ^{#1}	71.1(4)
O16-Zr3-O3 ^{#4}	72.3(3)	O11-Zr3-O15 ^{#1}	72.5(4)
O11-Zr3-O3 ^{#4}	74.0(4)	O5 ^{#3} -Zr3-O8	75.1(4)
O5 ^{#3} -Zr3-O3 ^{#4}	75.7(3)	O15 ^{#1} -Zr3-O8	76.3(4)
O10 ^{#1} -Zr3-O3 ^{#4}	76.9(3)	O11-Zr3-O5 ^{#3}	77.5(3)
O15-Zr3-O8	78.3(4)	O15 ^{#1} -Zr3-O5 ^{#3}	78.7(3)
O10 ^{#1} -Zr3-O16	89.1(4)	O15-Zr3-O16	89.6(4)

Symmetry codes for 493-MOF-BA: #1 = $x, -y + 3/2, -z + 1/4$; #2 = $-x, -y + 2, z$; #3 = $-x, y - 1/2, -z + 1/4$; #4 = $y - 1, x + 1/2, z - 3/4$. Symmetry codes for 493-MOF-TATB: #1 = $-x + 1/2, y, -z + 7/4$; #2 = $y, -x + 1, -z + 1$; #3 = $x - 1/2, -y + 1, -z + 7/4$; #4 = $-y + 1/2, -x + 1, z + 3/4$.

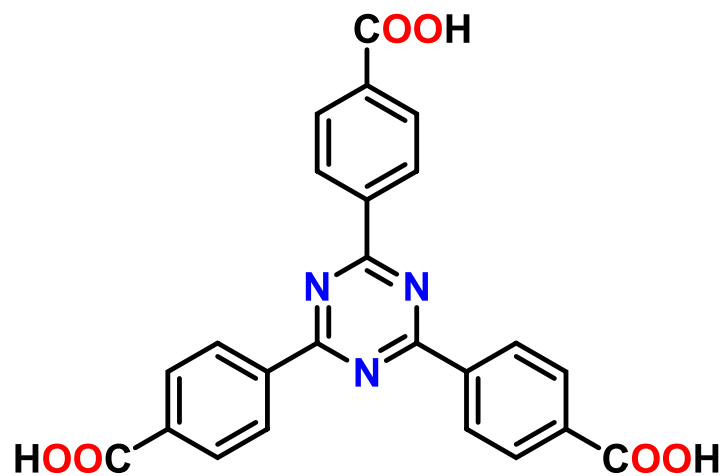


Fig. S1 Schematic drawing of the ligand H₃TATAB used in this work.

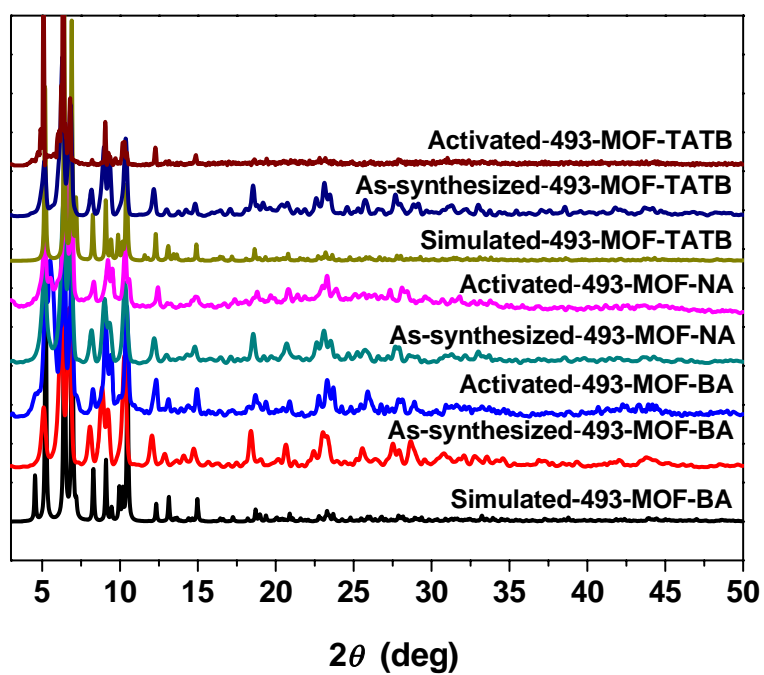


Fig. S2 PXRD patterns for simulated, as-synthesized, and activated 493-MOFs.

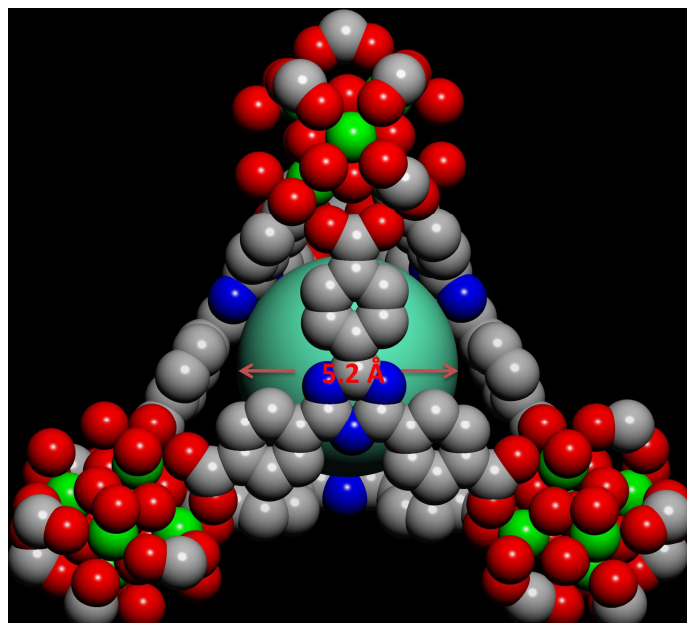


Fig. S3 View of the tetrahedral cage in 493-MOF-BA with the inner diameter of 5.2 Å.

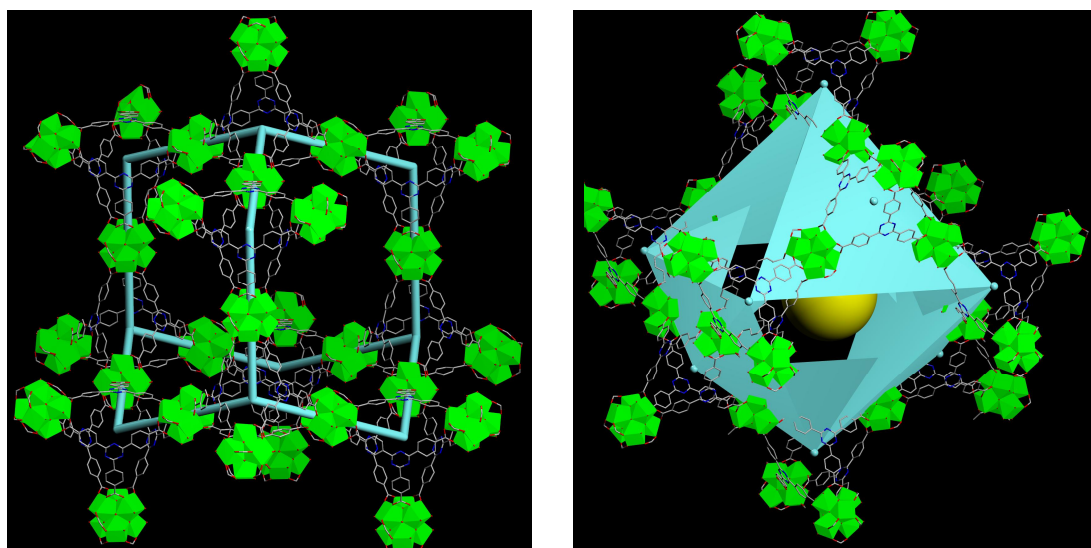


Fig. S4 The diamondoid mesoporous cage constructed by the linkage of tetrahedral microporous cages in 493-MOF-BA.

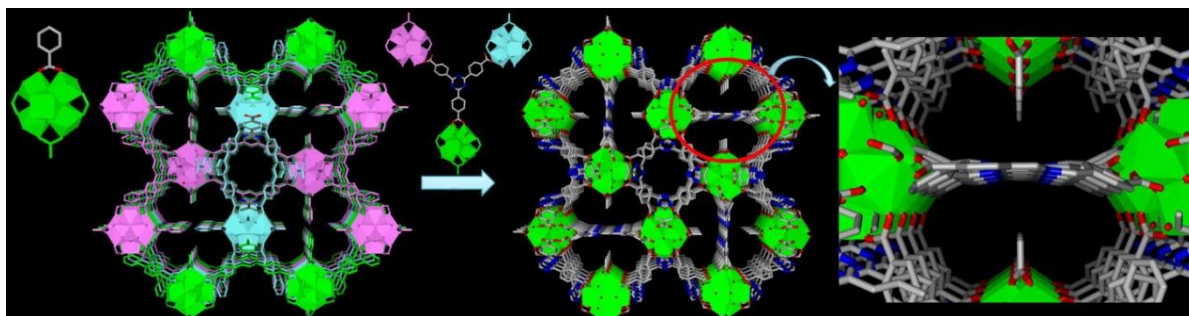


Fig. S5 The structural evolution from 493-MOF-BA to interrelated 493-MOF-TATB.

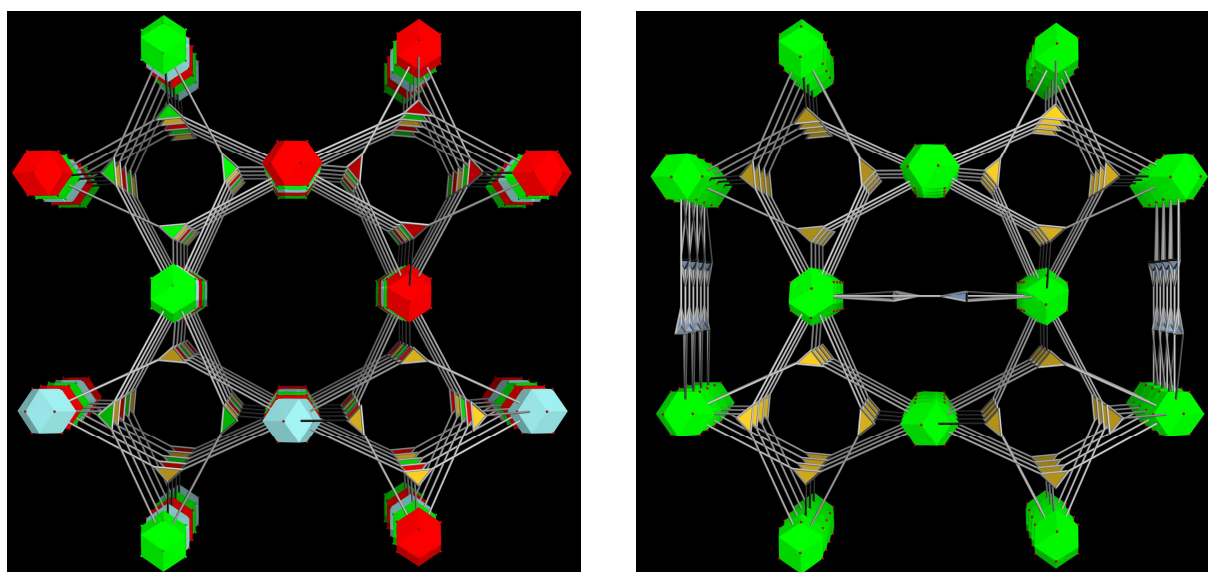


Fig. S6 The topological networks for (left) 493-MOF-BA and (right) 493-MOF-TATB.

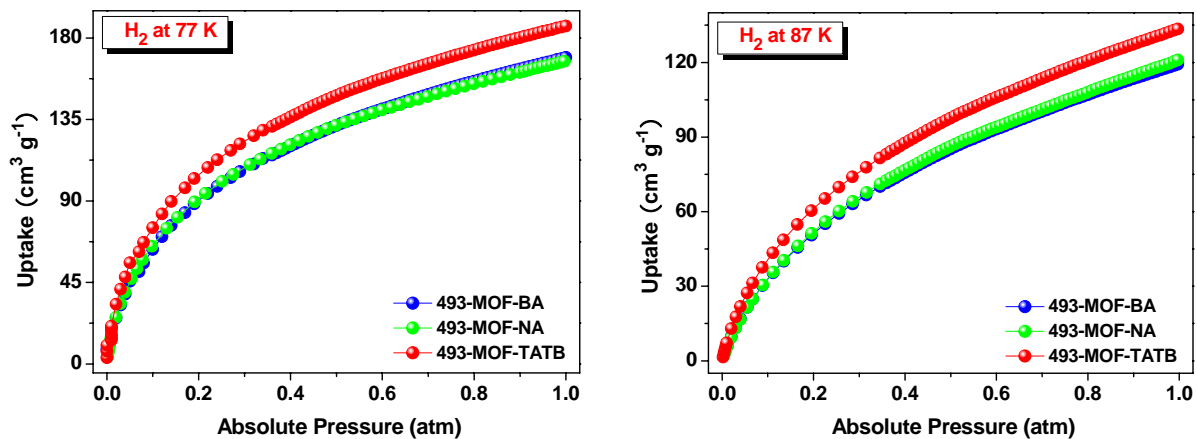


Fig. S7 Hydrogen sorption isotherms for activated 493-MOFs at 77 and 87 K.

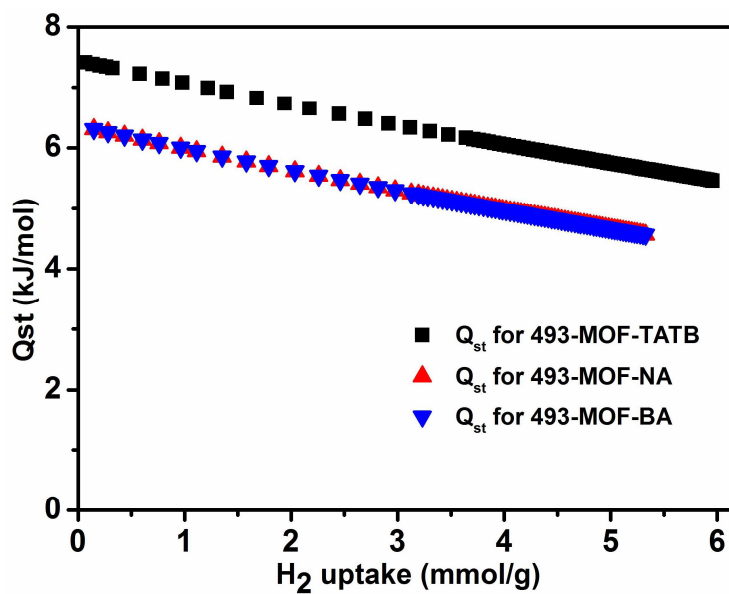


Fig. S8 The calculated H₂ sorption heats for activated 493-MOFs.

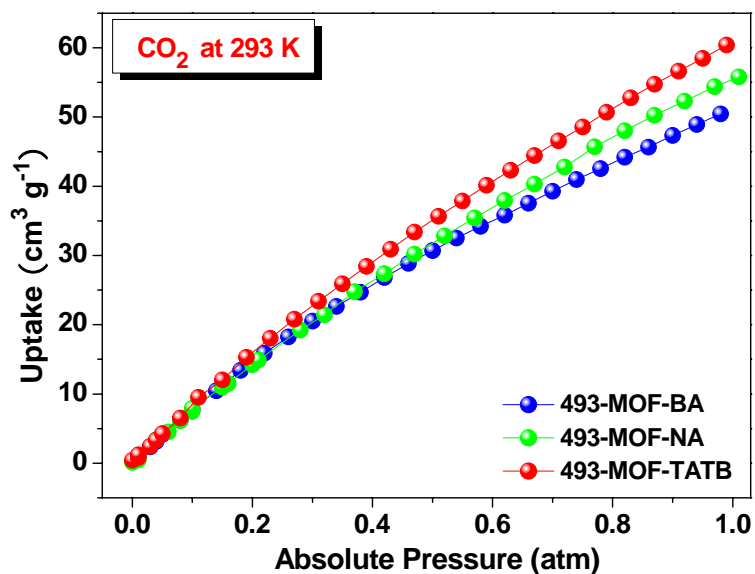


Fig. S9 CO₂ sorption isotherms for activated 493-MOFs at 293 K.

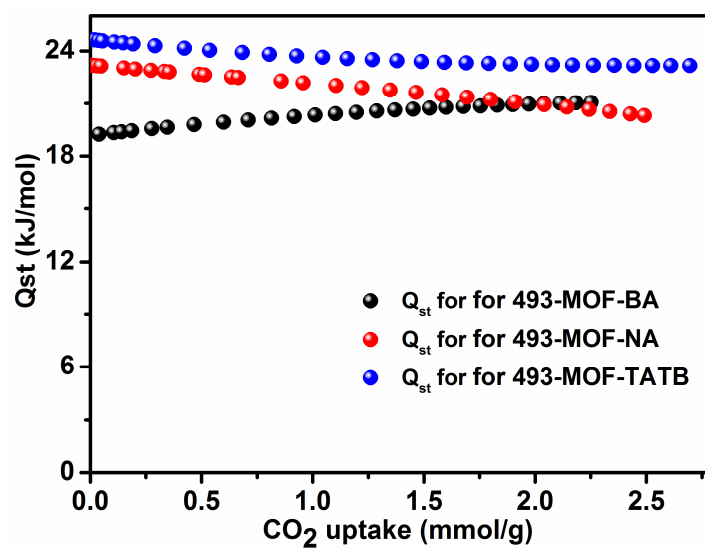


Fig. S10 The calculated CO₂ sorption heats for activated 493-MOFs.

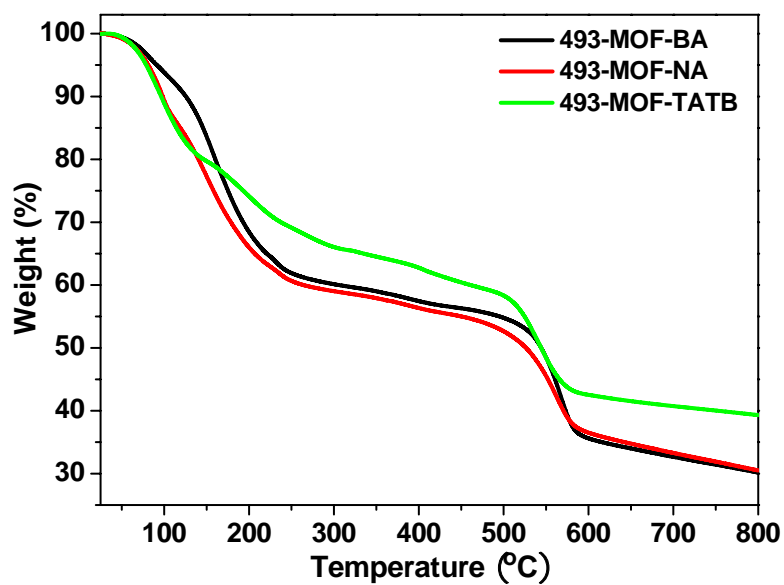
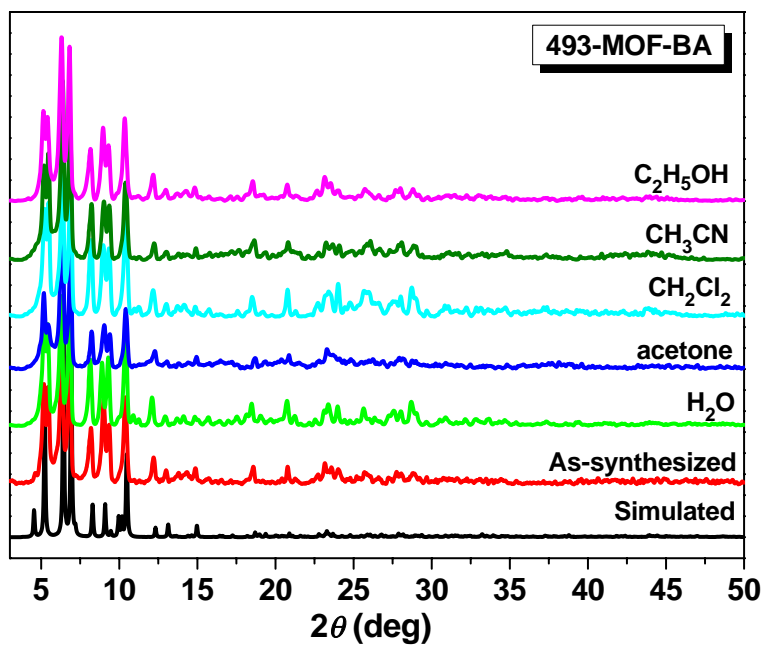


Fig. S11 TGA curves for 493-MOF-BA, 493-MOF-NA, and 493-MOF-TATB.



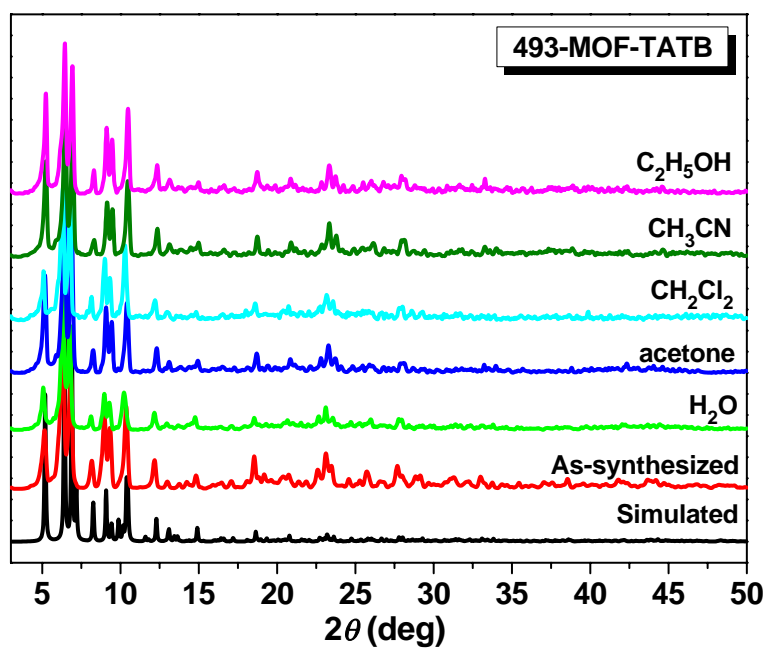
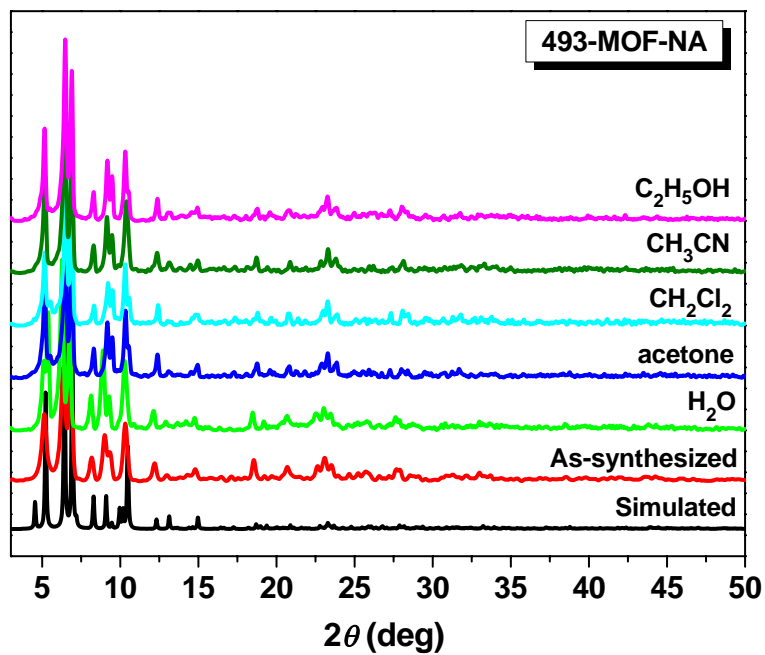
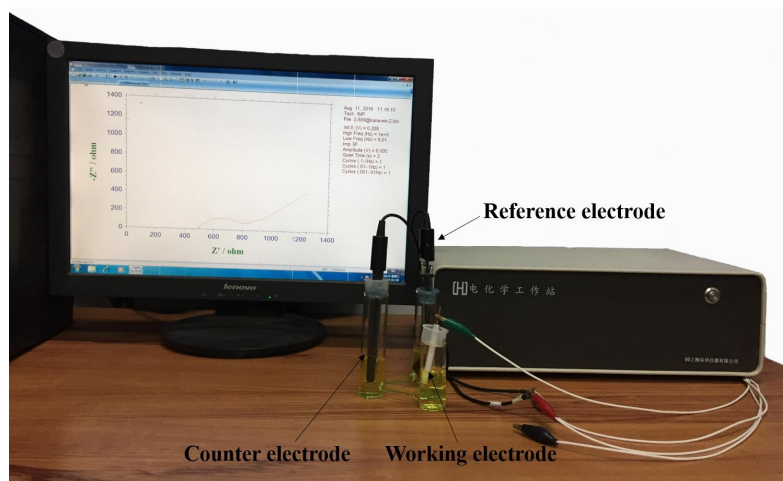
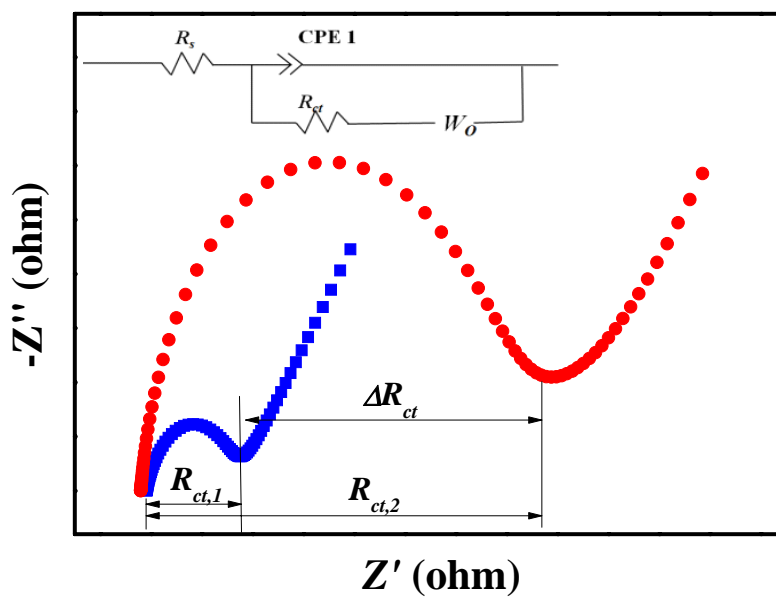


Fig. S12 PXRD patterns for 493-MOFs treated in organic solvents and water.



(a)



(b)

Fig. S13 (a) The setup for EIS measurements and (b) EIS Nyquist plots and equivalent circuit.

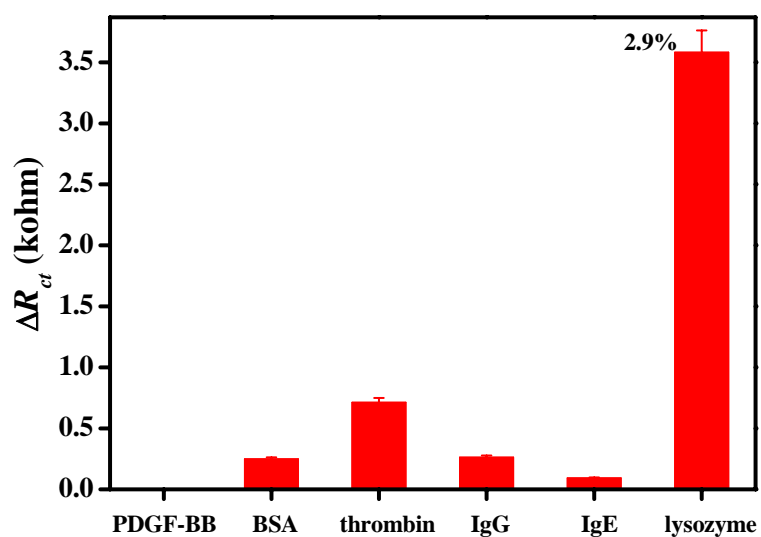


Fig. S14 Selectivity of 493-MOF-BA-based electrochemical aptasensor (histograms: the relative data of ΔR_{ct} and error bars: standard deviations of three replicate determinations).

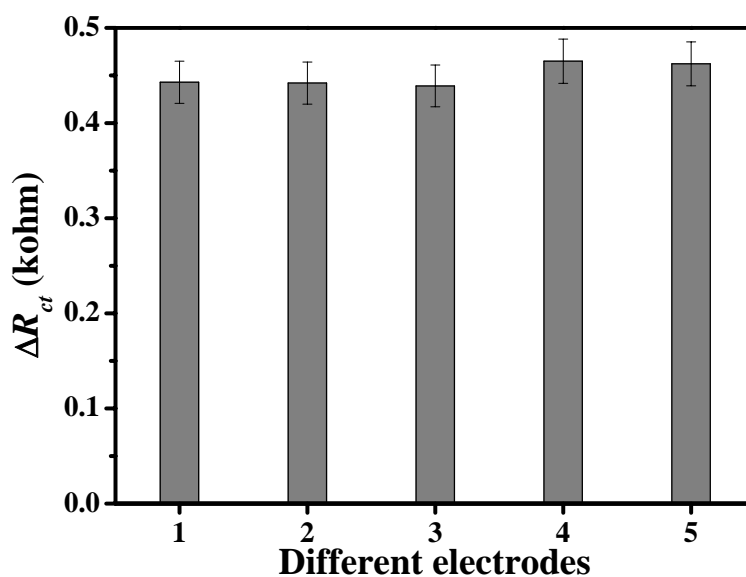


Fig. S15 Variations of ΔR_{ct} of five different electrodes modified with 493-MOF-BA.

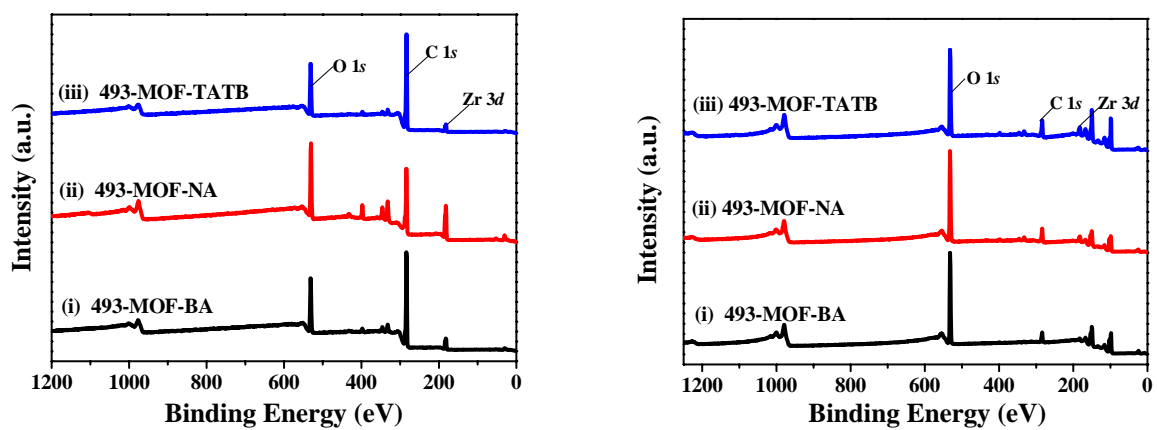


Fig. S16 XPS survey spectra for (left) 493-MOFs and (right) coated layers exposed to water.

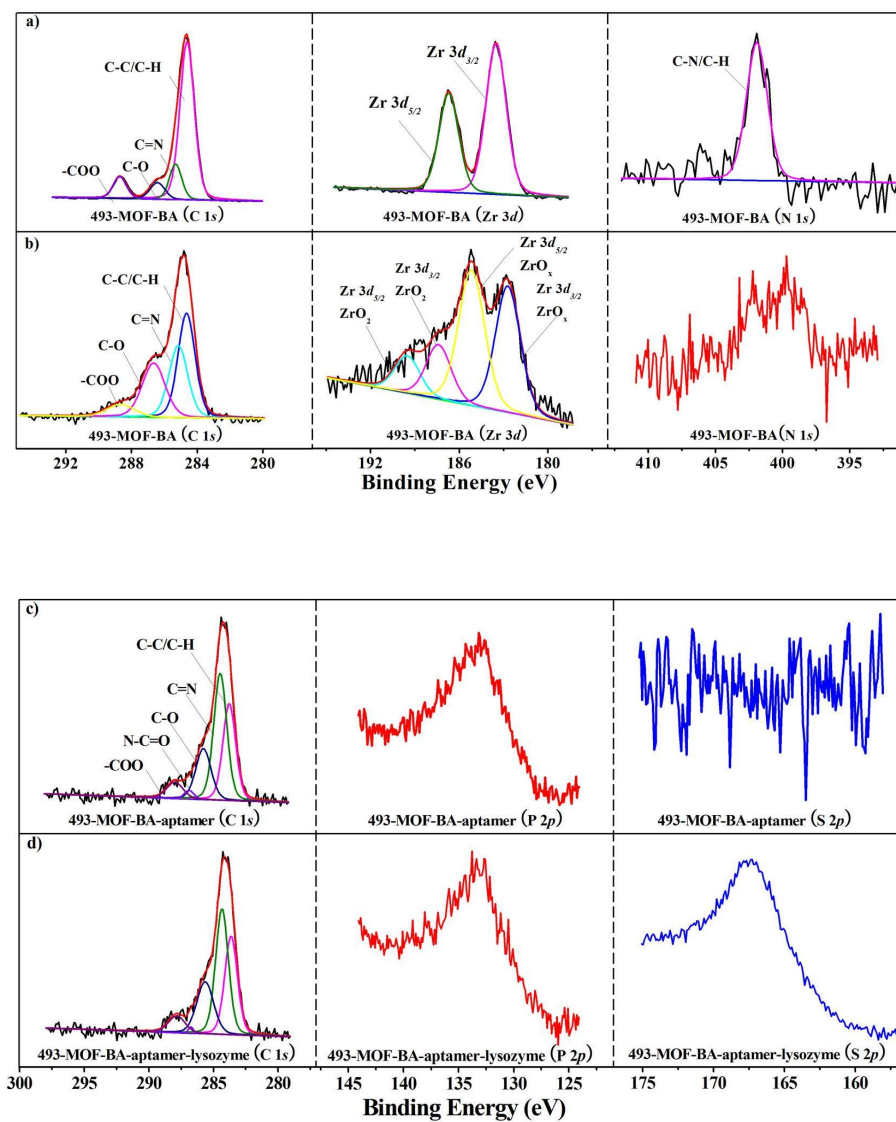


Fig. S17 XPS core-level spectra (C 1s, Zr 3d, and N 1s) for (a) 493-MOF-BA and (b) the coated layer exposed to water. XPS core-level spectra (C 1s, P 2p, and S 2p) for (c) 493-MOF-BA-aptamer and (d) 493-MOF-BA-aptamer-lysozyme.

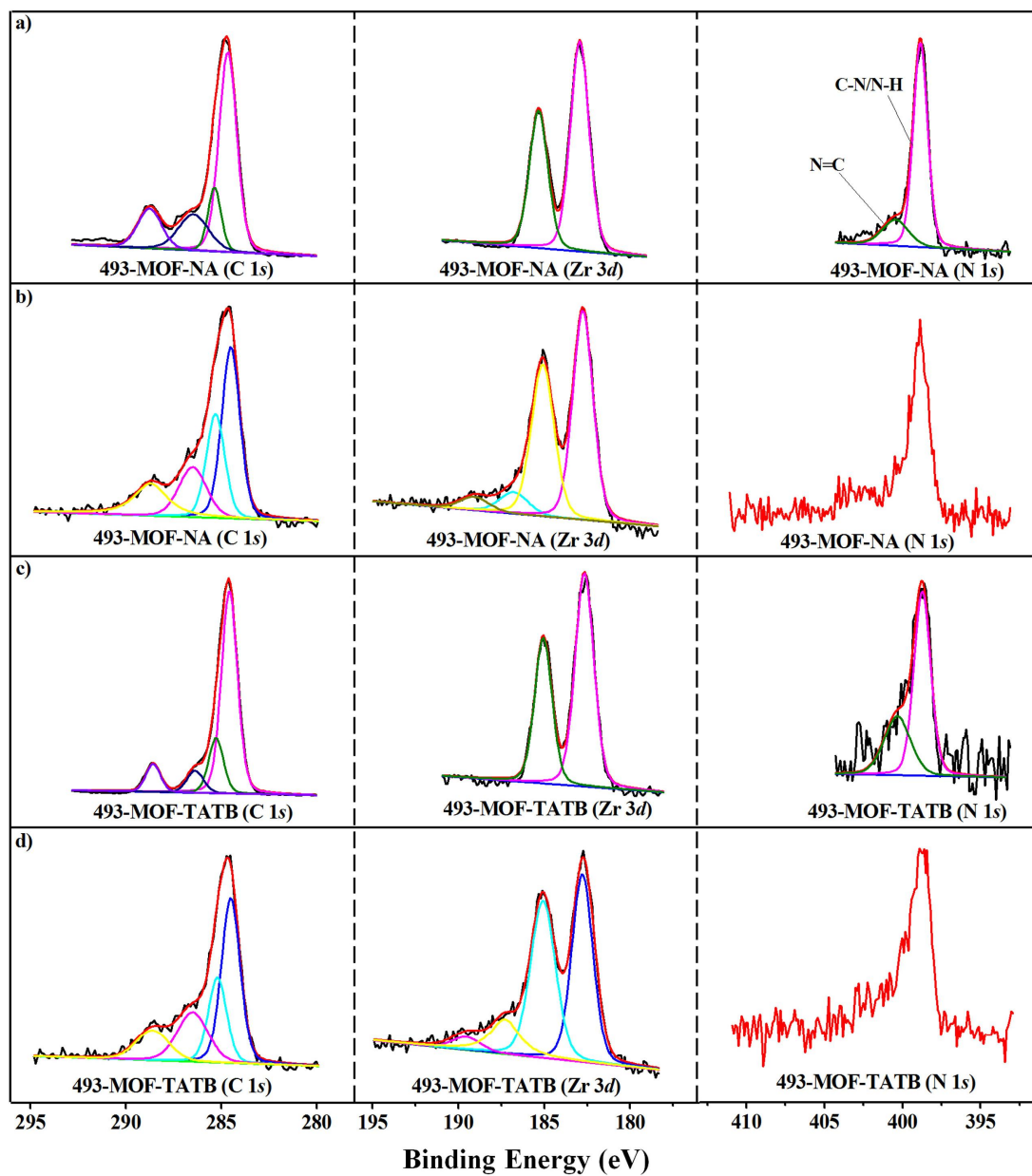


Fig. S18 XPS core-level spectra for (a) 493-MOF-NA, (b) 493-MOF-NA coated layer exposed to water, (c) 493-MOF-TATB, and (d) 493-MOF-TATB coated layer exposed to water.

Table S3 Comparison of the performances of electrochemical aptasensors for lysozyme detection.

Electrode materials	Technique	Linear range	LOD ^a	Reference
Versatile SPR aptasensor	SPR ^b	0.7–70 μ M	1.4 nM	S5
Luminescent G-quadruplex-selective iridium	Luminescence	2–50 nM	2 nM	S6
Aptamer-functionalized superparamagnetic nanoparticles	Magnetic relaxation switch	0.5–80 M	0.5 nM	S7
Iminodiacetic acid-Cu ²⁺ complex	EIS	0.1 pM – 0.1 mM	60 fM	S8
DNA duplex tagged with ferrocene	EIS	7–30 nM	0.45 nM	S9
Anti-lysozyme DNA aptamer	CV ^c	0–3.57 μ M	610 nM	S10
Plasm polymerization assisted composite of polyacrylic acid and hollow TiO ₂ spheres	EIS	3.57 pM – 7.14 nM	1.04 pM	S11
493-MOFs modified with aptamer	EIS	0.357–71.4 pM	0.26 pM	this work

^a LOD = Limitation of detection; ^b SPR = Surface plasmon resonance; ^c CV = Cycle voltammetry.

Table S4 The real samples determined by the fabricated aptasensor based on 493-MOF-BA.

Real samples	Amount added (ng mL ⁻¹)	Found (ng mL ⁻¹)	Recovery (%)	RSD% ^a
Serum	0.005	0.00586	117.2	2.3
	0.01	0.0094	94	4.5
	0.05	0.049	104.9	2.1
	0.1	0.098	98	1.5
	0.5	0.495	99	2.5
Wine	0.005	0.0052	104	3.2
	0.01	0.0099	99	3.1
	0.05	0.051	102	4.2
	0.1	0.13	103	1.5
	0.5	0.56	112	1.3
Egg white	0.005	0.0048	96	1.5
	0.01	0.00955	95	2.7
	0.05	0.053	106	3.5
	0.1	0.12	102	3.0
	0.5	0.498	99	3.3

^a RSD = Relative standard deviation.

Table S5 Atomic% of 493-MOFs and the coated layers exposed to water by XPS measurements.

Samples		Atomic (%)			
		C 1s	Zr 3d	N 1s	O 1s
As-synthesized	493-MOF-BA	76.96	1.27	2.81	18.96
	493-MOF-NA	61.05	4.05	7.77	27.13
	493-MOF-TATB	78.57	0.85	2.87	17.71
Coated Layers	493-MOF-BA	24.8	1.25	2.03	71.92
	493-MOF-NA	30.46	1.85	2.42	65.27
	493-MOF-TATB	33.87	2.59	3.6	59.94

Table S6 Atomic% of 493-MOF-BA, 493-MOF-BA-aptamer, and 493-MOF-BA-aptamer-lysozyme.

Fabrication Process of Aptasensor	Atomic (%)					
	C 1s	O 1s	N 1s	Zr 3d	P 2p	S 2p
493-MOF-BA	24.8	71.92	2.03	1.25	---	---
493-MOF-BA-aptamer	19.91	71.36	1.67	1.27	5.78	---
493-MOF-BA-aptamer-lysozyme	37.69	48.19	2.38	0.71	3.53	7.49

Table S7 The calculated binding interactions between aptamer strands and 493-MOFs.

	493-MOF-BA	493-MOF-NA	493-MOF-TATB
Total energy (kcal mol ⁻¹)	13476.020807	13428.542052	130478.881954
Framework energy (kcal mol ⁻¹)	13523.543602	13520.432442	130351.242348
Aptamer energy (kcal mol ⁻¹)	191.438524	203.624189	166.444150
Interaction energy (kcal mol ⁻¹)	-238.961319	-295.514579	-38.804544

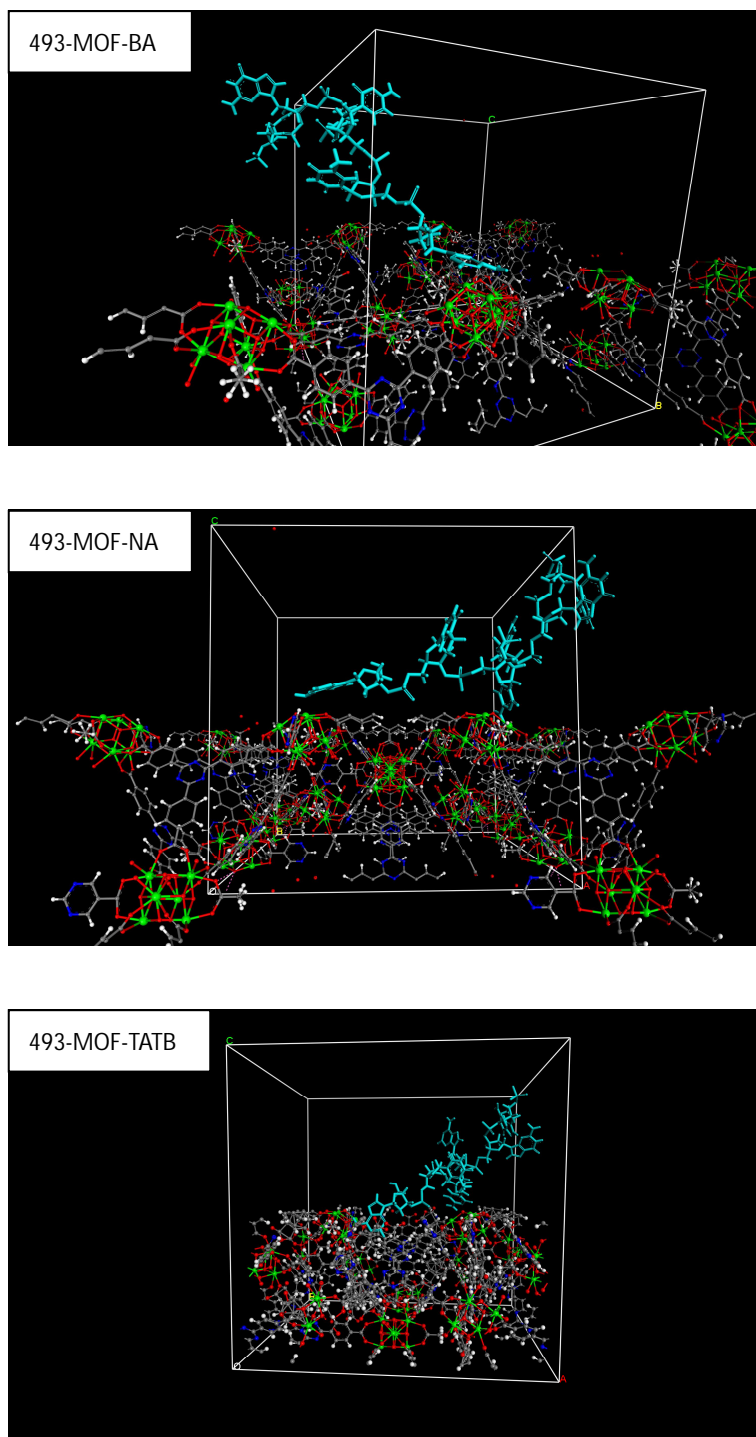


Fig. S19 The binding modes of aptamer strands with 493-MOFs simulated by Materials Studio 6.1.

References

- S1 G. M. Pogosyan, V. N. Zaplishnyi and I. A. Asaturyan, *Arm. Khim. Zh.*, 1977, **30**, 342–348.
- S2 *CrysAlis CCD and CrysAlis RED*, version 1.171.37.35, Oxford Diffraction Ltd: Yarnton, Oxfordshire, U. K., 2014.
- S3 (a) G. M. Sheldrick, *SHELXTL*, version 6.10, Bruker Analytical X-ray Systems: Madison, WI, 2001.
(b) G. M. Sheldrick, *Acta Crystallogr.*, 2008, **A64**, 112–122.
- S4 A. L. Spek, *J. Appl. Crystallogr.*, 2003, **36**, 7–13.
- S5 A. Vasilescu, C. Purcarea, E. Popa, M. Zamfir, I. Mihai, S. Litescu, S. David, S. Gaspar, M. Gheorghiu and J.-L. Marty, *Biosens. Bioelectron.*, 2016, **83**, 353–360.
- S6 L. Lu, W. Wang, M. Wang, T.-S. Kang, J.-J. Lu, X.-P. Chen, Q.-B. Han, C.-H. Leung and D.-L. Ma, *J. Mater. Chem. B*, 2016, **4**, 2407–2411.
- S7 S. Bamrungsap, M. I. Shukoor, T. Chen, K. Sefah and W. Tan, *Anal. Chem.*, 2011, **83**, 7795–7799.
- S8 A. Arabzadeh and A. Salimi, *Biosens. Bioelectron.*, 2015, **74**, 270–276.
- S9 Z. Chen and J. Guo, *Electrochim. Acta*, 2013, **111**, 916–920.
- S10 A. K. H. Cheng, B. Ge and H.-Z. Yu, *Anal. Chem.*, 2007, **79**, 5158–5164.
- S11 Z. Zhang, S. Zhang, L. He, D. Peng, F. Yan, M. Wang, J. Zhao, H. Zhang and S. Fang, *Biosens. Bioelectron.*, 2015, **74**, 384–390.